Towards single-photon Brillouin optical time domain reflectometry

Maxime Romanet,[1,*] Luis Miguel Giraldo,[1] Maxime Zerbib,[1] Etienne Rochat,[2] Kien Phan Huy,[3] Jean-Charles Beugnot,[1]

[1] *Université de Franche-Comté, CNRS, Institut FEMTO-ST, F-25000 Besançon, France*
[2] *Omnisens S.A, Morges, Switzerland*
[3] *SUPMICROTECH, Université de Franche-Comté, CNRS, institut FEMTO-ST, F-25000 Besançon, France*

[*] *Corresponding author: maxime.romanet@femto-st.fr*

Abstract: We investigate a novel distributed Brillouin optical time domain reflectometer (BOTDR) using standard telecommunication fibers based on single-photon avalanche diodes (SPADs) in gated mode, $\nu-$BOTDR, with a range of 120 km and 10 m spatial resolution. We experimentally demonstrate the ability to perform a distributed temperature measurement, by detecting a hot spot at 100 km. Instead of using a frequency scan like conventional BOTDR, we use a frequency discriminator based on the slope of a fiber Bragg grating (FBG) to convert the count rate of the SPAD into a frequency shift. A procedure to take into account the FBG drift during the acquisition and perform sensitive and reliable distributed measurements is described. We also present the possibility to differentiate strain and temperature.

1. Introduction

Brillouin scattering based distributed optical fiber sensors have become essential tools for civil engineering applications such as monitoring of pipelines or submarine cables [1,2]. Their field of application has expanded opening up new horizons for geophysicists and natural scientists [3–5]. These sensors, which take advantage of the frequency dependence of Brillouin gain on temperature and strain, fall into two categories [2, 6]. Brillouin optical time domain analysis sensors (BOTDA) use stimulated Brillouin scattering and require access to both ends of the fiber. Brillouin optical time domain reflectometers (BOTDR) that measure spontaneous Brillouin scattering require access to only one end of the fiber and provide a clear advantage in terms of simplicity. Increasing signal-to-noise ratio (SNR) represents a major challenge for these sensors. It determines the range of the sensor, typically 75 km on commercial devices. Increasing the range of BOTDR sensors makes it possible to contribute to the ecological transition, by helping to guarantee the integrity of submarine electrical cables for offshore wind farms. Numerous improvements have been proposed in terms of probe light [7, 8], remote amplification with Raman [9–11] or EDFA amplifiers [12, 13] or coding strategies [14–16]. The current range of BOTDR sensors is 100 km with Polarization-Diverse Coherent Detection [17], and 250 km combining Raman amplification and an EDF after few kilometers [18]. The former achieves 100 km temperature measurement with a straightforward design but also a signal-to-noise ratio degraded after 80 km. The latter, along with most recent improvements involves adding amplifiers within the fiber network or added complexity to the BOTDR setup.

Eventually, the signal-to-noise ratio (SNR) of the photodetector always limit the ultimate performance. With the development of quantum technologies, new detectors such as single-photon avalanche diodes (SPADs) and superconducting nanowire single-photon detectors (SNSPDs) become available [19]. They have shown their efficiency in many OTDR applications, improving sensing range while maintaining a good resolution [20–23]. They have also been used in distributed temperature sensors (DTS) using Raman backscattering, with a range of 50 km [24], and achieve spatial resolution of the order of a centimeter [25, 26]. They are thus good candidate to help developping a class of new devices, single-photon Brillouin optical time domain reflectometers ($\nu-$BOTDR), that could complement the traditional BOTDRs.

However, few studies have been carried out on $\nu-$BOTDR. They use either the Landau-Placzek ratio (LPR) requiring Rayleigh and Brillouin intensity measurements, to determine the temperature [27] or a scanning Fabry-Perot interferometer to scan the Brillouin resonance [28]. Measurements were reported up to 50 km with an estimated range of 90 km [28]. Therefore, numerous questions are left to be addressed to build a $\nu-$BOTDR such as range improvement, retrieving temperature information or ability to discriminate temperature from strain.

In this paper, we investigate a single-photon ν-BOTDR setup to perform distributed temperature measurements using a narrow fiber Bragg grating (FBG) without frequency scan. This idea has already been used in schemes

using traditional detectors with Mach-Zehnder interferometers as discriminators [29]. In particular, our configuration allows any instability issue to be addressed with a simple post-processing of the data. In the first section, we will present our experimental setup and demonstrate its detection range. Then, we will explain the principle of temperature measurement with a narrow FBG used as a frequency discriminator and show our experimental results. In the third section, we will show how instabilities can be corrected through real-time monitoring and post-processing of the data, thus eliminating the need for a feedback loop. Finally, we will give an overview of how our setup can deal with temperature-strain cross-sensitivity.

2. Measurement setup and sensing range

Our experimental setup is shown in Fig. 1 (top). A tunable narrowband laser (Apex technologies) sends light signal at $\lambda = 1547$ nm into a polarization controller (PC). The light is split in two beams by a 90/10 coupler. The beam with 10% of the light reaches an optical isolator (ISO) and a semiconductor optical amplifier (SOA) that shapes the pump pulses. Pulses go through a second optical isolator and an optical circulator (C1) before entering the fiber under test (FUT): a 120 km single-mode fiber (G625D). In order to carry out measurements automatically, all components are controlled by a computer.
Within the FUT, the light experiences spontaneous Brillouin scattering. It is scattered by thermally excited phonons that propagate along the fiber. The back-scattered light is shifted in frequency by the Doppler effect. The frequency shift is related to the acoustic velocity in the optical fiber, which depends on the temperature and the strain. The back-scattered light returns to the circulator C1 where it is routed towards an optical switch SW1. In *measurement mode*, the backscattered light is sent through SW1 to a circulator C2 and a narrow Fiber-Bragg Grating (FBG) that serves as a frequency discriminating reflector. Then the filtered backscattered light reaches a second switch SW2. SW2 carries the backscattered photons to an infrared SPAD from Auréa Technology operated in the so-called gated mode or Geiger mode. The applied bias is above the breakdown voltage, in order to have sufficient gain to be able to detect a single incident photon. The SPAD is based on InGaAs/InP, cooled around -50°C.

In order to make a distributed measurement along the optical fiber, it is important to locate precisely the position at which the light was backscattered; this is achieved by a time-of-flight measurement. As shown in Fig. 1 (top), by controlling the time delay Δt between the launch of the pulse from the SOA (blue 1) and the activation gate of the SPAD (pink 2), we can carry out measurements at a particular distance d:

$$\Delta_t = \frac{2d}{c} n_{SMF} + t_{setup} \tag{1}$$

where c is the speed of light in vacuum, n_{SMF} is the fiber refractive index, d is the sensing distance, t_{setup} is the delay due to propagation time in setup components (isolator, circulators, switch, patch cords, filter) and Δt is the photon round trip time of flight in the fiber under test (FUT).

The main advantage of using SPADs over conventional detectors is to increase the sensing range of the distributed sensor, which is determined by the signal-to-noise ratio (SNR) of the whole setup. In our case, the SNR is the ratio between the measured Brillouin anti-Stokes signal and the noise level on the SPAD. The strength of the Brillouin anti-Stokes signal is determined by the peak power of the SOA pulses, the losses in the optical fiber and components, the Brillouin scattering efficiency and the detection efficiency of the SPAD. The noise on the SPAD is made up of two types of noise, the optical noise from the setup, and the intrinsic noise of the SPAD. The optical noise is related to the optical signal coming from the setup. It is determined by three factors. First, the extinction rate of the SOA defines the background noise between the pulses. This noise can eventually reach the SPAD and trigger unwanted photon counts. Then, the cross-talk of the circulators C1 and C2 quantifies the signal that leaks from the SOA directly to the SPAD without going through the fiber under test. Finally, the filter efficiency gives the rejection efficiency of the Rayleigh, Brillouin Stokes and Raman backscattering. The second is the intrinsic noise of the SPAD, called dark count rate (DCR), which depends on the efficiency, the dead time and the duration of the gates set on the SPAD. As a consequence, careful attention has been given to the setup to provide the best SNR with the available components, and also to the SPAD parameters chosen in order to limit the DCR and avoid after pulsing. These parameters are specified in the table in Fig. 1 (bottom).

Using the specifications in Fig. 1 (bottom), we can predict the detection rate:

$$C_{,cps} = \eta_s \frac{\tau}{T} \frac{S_{B,W}}{\omega} \quad , \tag{2}$$

Where is the reduced Planck constant, ω is the pulsation of light, η_s the SPAD efficiency, τ the gate duration of the SPAD, T the period and $S_{B,mW}$ the backscattered Brillouin power [mW] defined as:

$$S_{B,mW} = 10^{\frac{S_{B,dBm}}{10}}, \quad [\text{mW}] \tag{3}$$

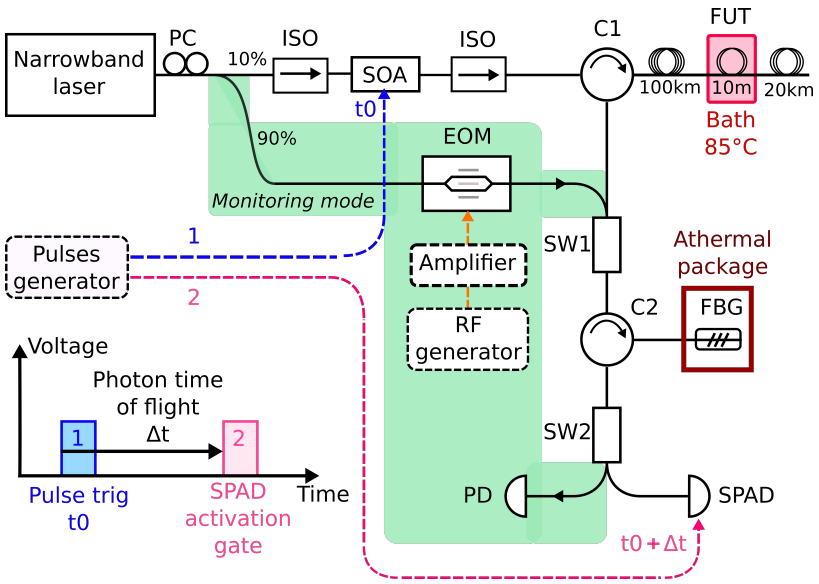

Laser	Emission wavelength for measurements	1547.8 nm
	Tunability range	1550 ± 20 nm
	Tunability resolution	1 pm
	Output power *	+11 dBm
SOA	Input power *	0 dBm
	Pulse peak power, P_{peak} *	+15 dBm
	Pulse extinction ratio *	62 dB
	Pulse width *	100 ns
	Pulse period, T *	1.25 ms
Circulator	C1 isolation/crosstalk *	62 dB
	C2 isolation/crosstalk *	51 dB
Fiber	G.652.D optical fiber, α_{SMF} *	0.19 dB/km
FBG	Insertion losses, α_{FBG} *	2.5 dB
	Line width (FWHM) *	2.7 GHz
	Rayleigh Attenuation (11 GHz from working point) *	42 dB
SPAD	Efficiency, η_s *	20 %
	Dark count, D_k (free-running) **	$\leq$ 1150 cps
	Dead-time **	20 μs
	Gate, τ *	50 ns
	Dark count d_k in our gated setup *	0.0437 cps

Fig. 1. (top) Experimental setup. Green area: FBG frequency response monitoring. PC: Polarization controller, ISO: Optical isolator, SOA: Semiconductor Optical Amplifier, EOM: Intensity Electro-Optic modulator, C1-C2: circulators, FUT: Fiber under test. Red area: Temperature controller bath (T = 85 °C). SW1-SW2: Optical switches, FBG: athermal packaged Fiber Bragg Grating, SPAD: Single-Photon Avalanche Diode, PD: Photodiode. Dash line: electrical cables. (bottom) Component specifications. $*$ Measured, $**$ Given by manufacturer test report.

The backscattered Brillouin power along the fiber is defined as:

$$S_{B,dBm} = P_{\text{peak}} - g_B - 2\,d\,\alpha_{SMF} - \alpha_{setup}, \quad [\text{dBm}] \tag{4}$$

where P_{Peak} is the pulse peak power injected in the fiber, g_B is the Brillouin efficiency (78 dB in our configuration), d is the probed distance [km], α_{SMF} are fiber losses and α_{setup} are components losses of the setup (circulators, filter, switch).

The experimental results are presented in Fig. 2. The Brillouin anti-Stokes count rate is reported in count per second (cps) with a logarithmic scale as a function of the probed distance.

The low noise level of the sensor (0.05 cps), represented in blue on Fig. 2 allows us to reach a distance up to

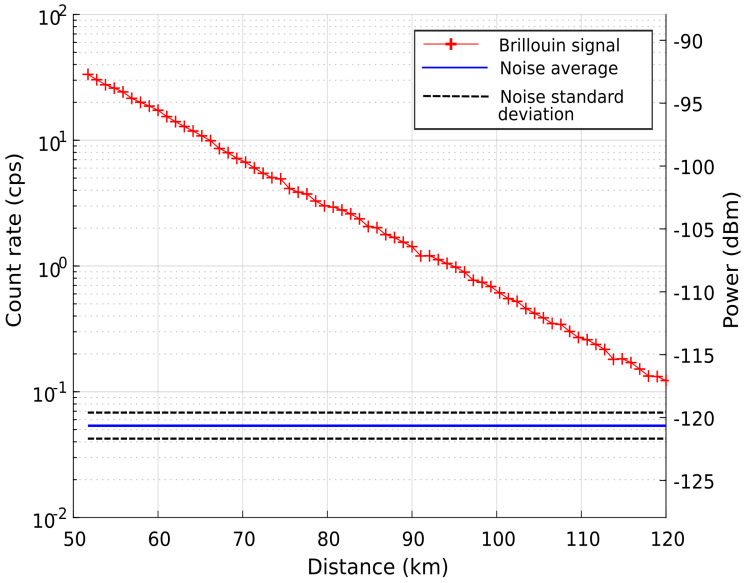

Fig. 2. (Red) ν-BOTDR trace from 50 km to 120 km realized with operating point A (see Fig. 3), with a 10 m spatial resolution (SOA 100 ns pulse width), 50 ns SPAD gates. (Blue) Noise floor average. (Dark dotted) Noise floor standard deviation.

120 km, with a 10 m spatial resolution, which is 30 km longer than the results reported in [28]. On Fig. 2 we only measure from 50 km where current commercial devices start to be less efficient.

These results could be further improved by increasing the signal-to-noise ratio (SNR) of the setup. For example, only +15 dBm power is launched into the fiber while commercial devices commonly use +23 dBm. Similarly, using a SNSPD, one could improve the SNR by 20 dB [30]. In theory with proper components such a setup could then reached over 190 km, approaching the performance obtained with a $\nu - OTDR$, using a SNSPD, with a range of 217km [23]. The difference between the theoretical range of our setup and the range of ν-OTDR is simply due to the higher efficiency of Rayleigh backscattering. In this article, at 120 km, the sensor still has a signal-to-noise ratio (SNR) of 3.6 dB, which is a first step in the demonstration of a $\nu-$BOTDR.

3. Temperature measurements

BOTDR sensors use the Brillouin frequency shift, to measure the temperature along an optical fiber. Usually, a heterodyne setup with a local oscillator is used. Such a configuration is not allowed in our case because the local oscillator would blind our single-photon detector. In our experiment, we develop a frequency discriminator. This allows us to transform a frequency variation into an intensity variation. The frequency discriminator is the slope of a narrow FBG that gives access to the Brillouin frequency. The FBG frequency response is shown in Fig. 3, where the linear area of the slope (over 576 MHz) is represented in red. From the frequency shift, we can deduce the temperature shift with the temperature sensitivity coefficient $C_{\nu_B T}$ = 1.07 MHz/K for a step index single-mode fiber at 1550 nm [2]. Thanks to this method, we only need to set the frequency laser to the desired working point shown in Fig. 3, and during the measurement we do not need to make a frequency scan of the Brillouin response. By avoiding the frequency sweep, we also reduce the measurement time.

It shows that, for an operating point halfway down the left-hand slope of the transmission band, we get 5% transmission variation for 42 MHz frequency shift. This ratio η_c = 8.2 MHz/% enables to turn a frequency shift variation into a count rate variation on the SPAD. In order to perform distributed temperature measurement, the propagation losses shown in Fig. 2 must be removed. Count rate datas are thus processed in order to compensate for the fiber losses, as a function of the probed distance, as depicted in Fig. 5.

In Fig. 4 (a), we report the temperature measurement obtained this way at operating point A (see Fig. 3) from a 10 m sample of a fiber immersed in $85 \pm 1.5\ ^\circ C$ water after 100 km.

We demonstrate the ability to detect a hot point of 10 m, at 100 km, with 100 ns optical pulses. The profile is realized with a sampling interval of 2.5 m. In gated mode, the sampling interval corresponds to the time delay between two active gates on SPAD. At this distance, we get a count rate of 0.55 count per second (cps), cor-

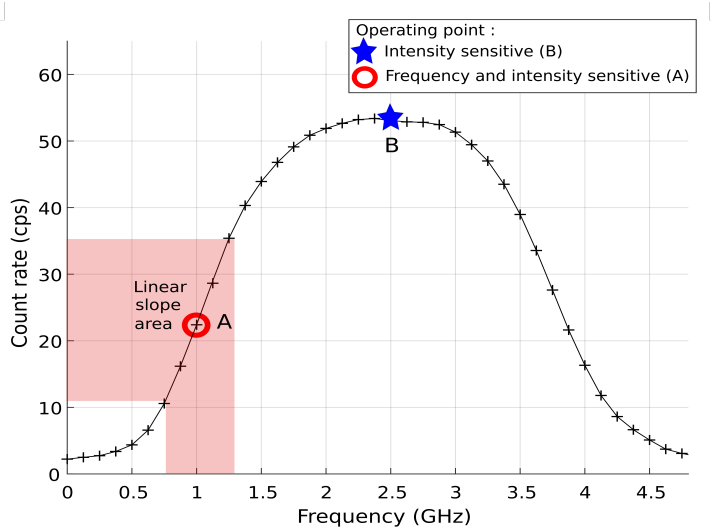

Fig. 3. Frequency response of our narrow FBG, scanned with SPAD, with an acquisition times equal to 60 s. Red circle: operating point A for frequency measurement. Blue star: operating point B, for intensity measurement only. The portion of the slope highlighted in light red indicates the area in which the response is linear, with a maximum deviation of 10% from linearity. It extends over 576 MHz.

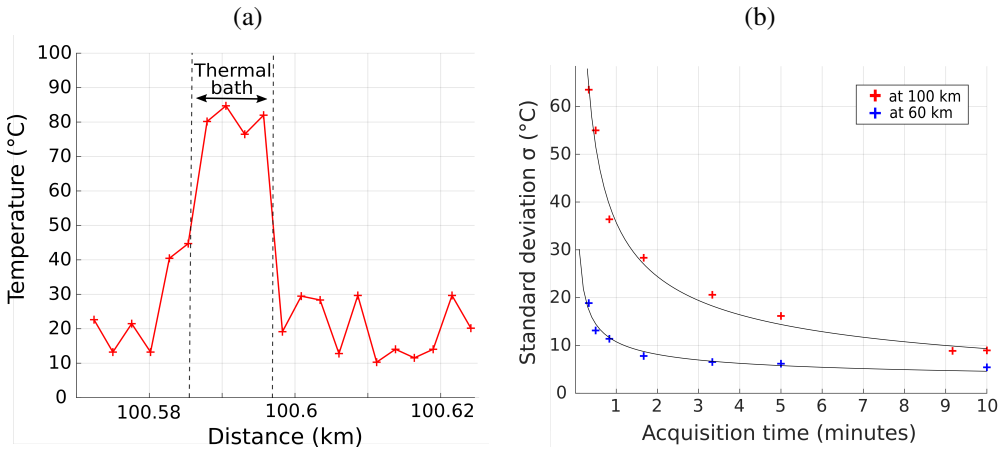

Fig. 4. (a) Measured temperature profile between 100.57 km and 100.63 km, with 10 m fiber spool in bath at $85 \pm 1.5°C$. Operating point A (see Fig. 3) was used with a 10 m spatial resolution and 10 minutes acquisition times. (b) Standard deviation of the temperature measurement as a function of the acquisition time, by repeating 10 times each measurements, at 60 km in blue and at 100 km in red.

responding to a SNR of 10.4 dB. The points measured at 45 °C outside the bath simply correspond to samples overlapping the thermal transition, linked to a spatial resolution of 10 m. Moreover, the jitter delay line of 1.5 ns adds uncertainty to the sampling. In Fig. 4 (b), we present the standard deviation on 10 consecutive temperature measurements according to the acquisition time at 60 km and 100 km. We demonstrate experimentally a standard deviation of $\sigma_{100km} = 8.9°C$ at 100 km and $\sigma_{60km} = 5.4°C$ at 60 km, with an acquisition time of 10 minutes for both distances. The difference of the standard deviation between the 2 distances is explained by the higher level of signal at 60 km (+15.2 dB compared to 100 km), giving a better statistic and higher number of events. One can also see that for sufficient time acquisition, the standard deviation reaches an optimum that defines the temperature resolution. Even if we use the FBG slope to avoid a frequency scan, the acquisition time is quite long compared to conventional BOTDR. This is due to an acquisition point per point along the optical fiber which is intrinsic to the gated mode of the SPAD. This measurement confirms the narrow FBG as a valid frequency discriminator, to convert count rate variation into temperature measurements. A more detailed reduction of acquisition time

measurement of our $\nu-$BOTDR is the subject of a future work.

4. Real-time monitoring and data post processing

The use of a frequency discriminator such as a narrow FBG has an obvious disadvantage. The relative frequency deviation between the laser and the FBG frequency is expected to be perfectly stable. Such setup will be sensitive to any form of instability (laser drift, high temperature variation). It thus usually requires a feedback loop to be reliable at the cost of increased complexity. However, this is not necessary in our case if we take advantage of the statistical nature of single-photon measurements. Indeed, the conversion of the count rate into Brillouin frequency shift is done by knowing the slope of the FBG at the given operating point. This operating point varies with the relative frequency difference between the laser and the FBG frequency. By measuring this difference, a new operating point can be deduced and the Brillouin frequency shift calculated with an updated conversion parameter η_c. Since single-photon detectors record events, it is only necessary to apply the measured relative frequency position of the FBG on experimental data in order to correct the drift as shown in Fig. 5. To achieve this, first we use a FBG with an athermal package in order to prevent thermal shocks and rapid temperature variations, leaving only slow temperature drifts (>10 min). Every 10 minutes, the setup switches to *monitoring mode* and the relative deviation between the laser and the FBG is monitored using the part of the setup highlighted in green in Fig. 1. Switches SW1 and SW2 are then used to take some of the light from the laser and pass it through an EOM modulator. The modulator produces a frequency-adjustable harmonic that probes the FBG filter at 11 GHz. A frequency sweeping of the laser allows scanning the FBG, and the transmission is measured by the photodiode PD. Thus, FBG frequency shift with respect to the laser frequency is measured. The position of the operating point at 11 GHz of the laser frequency for a temperature of 300 K can be computed (red area on Fig. 3). If the FBG has drifted with respect to the laser, the slope at the operating point is measured and the following registered single-photon detections will be post processed accordingly as shown in green in Fig. 5.

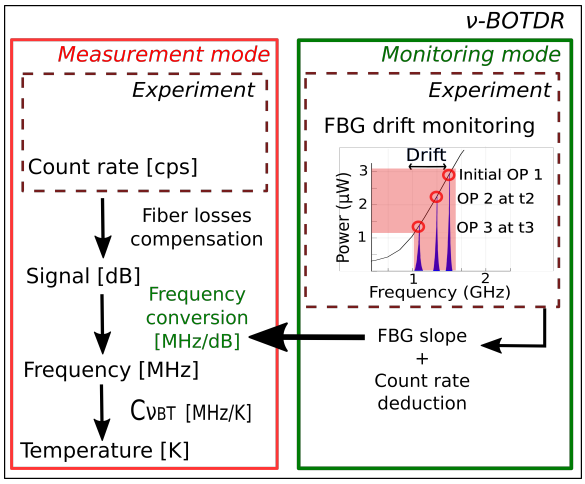

Fig. 5. Bloc diagram explaining the real-time monitoring of the $\nu-$BOTDR. In red, the data processing of the *measurement mode* is explained. In green, the *monitoring mode* is shown. It allows scanning the FBG shift every 10 minutes, in less than 1 minute, in order to compute the new operating point (OP) and the FBG slope. The Brillouin anti-Stokes resonance is represented in blue on the diagram. The contribution of the new operating point to the statistical measurement of the Brillouin frequency shift is corrected accordingly.

Thanks to the FBG scanning, it is possible to compensate for filter drift, and thus to correct frequency measurements thanks to a dedicated post-processing. Note that this does not add complexity to the detection setup since single-photon measurement is inherently statistical. Single-photon detection requires the electronics to record an event for each detected photon and then calculate the average photon flux. Adding additional processing to this calculation step is of negligible cost, while the lack of a feedback loop makes the setup simple and robust in *measurement mode*. Standard BOTDR setup usually requires an optoelectronic setup to continuously scan the Brillouin frequency. Here the optoelectronic setup is only used to monitor the system. Similarly, any other environment monitoring measurement could be added to retain or discard specific recorded events and refine the measurement.

5. Towards cross-sensitivity measurements

One of the caveats of our setup is that the count rate we measure on working point A (see Fig. 3) depends on both the Brillouin frequency shift and the efficiency of the Brillouin scattering. Both varies with temperature and strain [2]. One way to overcome this problem is to perform an additional control measurement when a temperature variation is recorded. By setting the laser frequency to change the operating point to B in the middle of the FBG band pass filter as shown in Fig. 3, we only measure the efficiency of the Brillouin scattering. The superposition of both measurement are reported in Fig. 6, where the sensitivity is computed for the two methods.

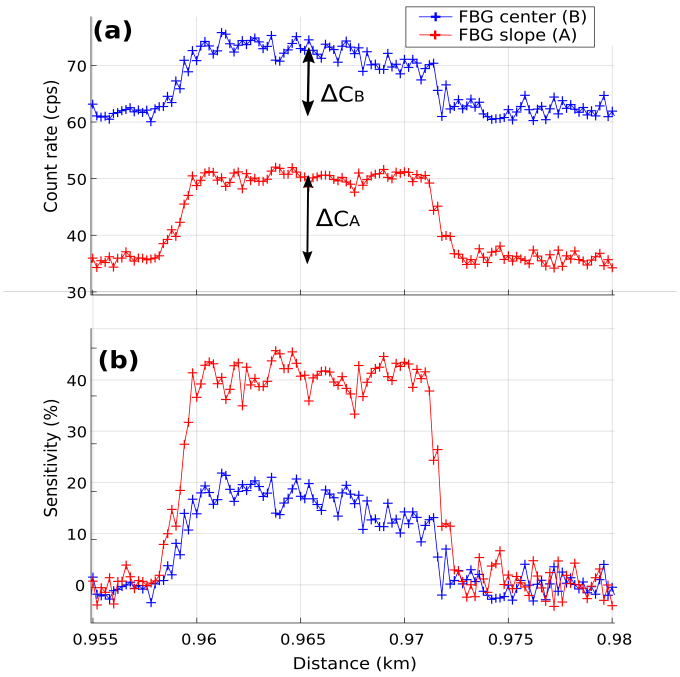

Fig. 6. Comparison of 2 working points A and B (see Fig. 3), with a 10 m fiber spool in bath at $84 \pm 1.5°C$, at 1 km, with 15 ns optical pulses. Blue: Measurements realized at operating point B. Red: Measurements realized at operating point A. (a) Original data measurement. (b) Sensitivity comparison of both methods, with a reference at ambient temperature between 975 m and 980 m by averaging counts on this area.

One can see in red the measurement with operating point A that includes both frequency shift and intensity contribution, while the measurement in blue only gives the intensity contribution. On Fig. 6 we show the sensitivity of both methods, defined as:

$$Sensitivity = \frac{Count\ rate}{\text{avg}(Count\ rate_{Ambiant})} \times 100 \quad [\%], \tag{5}$$

where $Count\ rate_{Ambiant}$ corresponds to the count rate averaging between 975 and 980 m, which is the reference level signal at room temperature. We clearly see that sensitivity at working point A, by using the slope of the FBG is higher (41%) than the B working point (16%) even if the count rate is lower for operational point A due to FBG losses. The highest sensitivity is obtained thanks to the frequency sensitivity ratio η_c linked to the slope. Thereby, our method demonstrates a better sensitivity compared to LPR method based on Brillouin and Rayleigh intensity measurements [28].

Similarly to [2], if we measure the count rate variation for a given temperature and strain variation for both A and B operating points, we can obtain the coefficients of the matrix M as seen on the right-hand side of:

$$\begin{aligned} \begin{pmatrix} \Delta C_A \\ \Delta C_B \end{pmatrix} &= \begin{pmatrix} a_{\Delta T,A} & a_{\Delta T,B} \\ a_{\Delta \varepsilon,A} & a_{\Delta \varepsilon,B} \end{pmatrix} \begin{pmatrix} \Delta T \\ \Delta \varepsilon \end{pmatrix}, \\ &= M \begin{pmatrix} \Delta T \\ \Delta \varepsilon \end{pmatrix}. \end{aligned} \tag{6}$$

By inverting this matrix, one can retrieve the temperature and strain from both count rates variation.

$$\begin{pmatrix} \Delta T \\ \Delta \varepsilon \end{pmatrix} = M^{-1} \begin{pmatrix} \Delta C_A \\ \Delta C_B \end{pmatrix} \tag{7}$$

Where ΔC_A and ΔC_B are respectively the count rate variation measured for working point A and B. The temperature shift coefficients $a_{\Delta T,A}$, $a_{\Delta T,B}$ and strain shift variation $a_{\Delta\varepsilon,A}$, $a_{\Delta\varepsilon,B}$ are related to temperature variation ΔT and strain variation $\Delta\varepsilon$ with (6).
A measurement at the working point A and B would allow performing temperature and strain measurements separately.

6. Conclusion

We have reported a $\nu-$BOTDR temperature measurement based on SPAD and a FBG frequency discriminator. The advantage of using SPADs for distributed sensor is the ability to measure small signal down to $-$ 120 dBm, without the need for a cryostat, unlike SNSPDs. The high signal-to-noise ratio (SNR) allows measuring the distributed Brillouin response up to 120 km with a spatial resolution of 10 m in standard single mode fiber. We demonstrate the ability to detect a hot spot at 100 km, and obtain a higher sensibility using a FBG compared to the LPR method. Thanks to the monitoring mode, environmental instabilities can be taken care of without the need of a feedback loop or adding complexity to the detection setup. By using different operating points on the FBG we show the possibility to discriminate strain and temperature effect without measurement of the Rayleigh intensity. In the future, the signal-to-noise ratio offered by single-photon detectors can open new possibility to extend the measurement range of Brillouin sensor reflectometers. Such performances can be useful for monitoring long submarine power cables, when fiber loop are not available and where no power is available along the fiber to amplify the optical signal. This new device might thus help with the ongoing ecological transition.

Funding

The authors would like to acknowledge the financial support of EIPHI Graduate School (contract ANR-17-EURE-0002), European ACTPHAST 4.0 project and French research ministry and SUPMICROTECH-ENSMM.

Acknowledgment

We thank Marc Niklès and Félix Bussières for fruitful discussions, Jean-Marc Merolla for helpful discussion and AUREA technology for support in SPAD.

Disclosures

The authors declare no conflicts of interest.

References

1. A. Motil, A. Bergman, and M. Tur, "State of the art of brillouin fiber-optic distributed sensing," Opt. & Laser Technol. 78, 81–103 (2016).
2. A. H. Hartog, An Introduction to Distributed Optical Fibre Sensors (CRC Press, 2017).
3. . B.-j. Wang, K. Li, B. Shi, and G.-q. Wei, "Test on application of distributed fiber optic sensing technique into soil slope monitoring," Landslides 6, 61–68 (2009).
4. Y. Yin, H. Wang, Y. Gao, and X. Li, "Real-time monitoring and early warning of landslides at relocated Wushan Town, the Three Gorges Reservoir, China," Landslides 7, 339–349 (2010).
5. L. Zeni, L. Picarelli, B. Avolio, A. Coscetta, R. Papa, G. Zeni, C. Di Maio, R. Vassallo, and A. Minardo, "Brillouin optical time-domain analysis for geotechnical monitoring," J. Rock Mech. Geotech. Eng. 7, 458–462 (2015).
6. Q. Bai, Q. Wang, D. Wang, Y. Wang, Y. Gao, H. Zhang, M. Zhang, and B. Jin, "Recent Advances in Brillouin Optical Time Domain Reflectometry," Sensors (Basel, Switzerland) 19, 1862 (2019).
7. C. Li, Y. Lu, X. Zhang, and F. Wang, "SNR enhancement in Brillouin optical time domain reflectometer using multi-wavelength coherent detection," Electron. Lett. 48, 1139–1141 (2012).
8. Y. Zhang, X. Wu, Z. Ying, and X. Zhang, "Performance improvement for long-range BOTDR sensing system based on high extinction ratio modulator," Electron. Lett. 50, 1014–1016 (2014).
9. Y. T. Cho, M. Alahbabi, M. J. Gunning, and T. P. Newson, "50-km single-ended spontaneous-Brillouin-based distributed-temperature sensor exploiting pulsed Raman amplification," Opt. Lett. 28, 1651–1653 (2003).
10. Y. T. Cho, M. N. Alahbabi, M. J. Gunning, and T. P. Newson, "Enhanced performance of long range Brillouin intensity based temperature sensors using remote Raman amplification," Meas. Sci. Technol. 15, 1548–1552 (2004).
11. M. Song, Q. Xia, K. Feng, Y. Lu, and C. Yin, "100 km Brillouin optical time-domain reflectometer based on unidirectionally pumped Raman amplification," Opt. Quantum Electron. 48, 30 (2015).

12. F. Gyger, E. Rochat, S. Chin, M. Niklès, and L. Thévenaz, "Extending the sensing range of Brillouin optical time-domain analysis up to 325 km combining four optical repeaters," in 23rd international conference on optical fibre sensors, vol. 9157, pp. 957–960. (2014).
13. P. Clement, R. Gabet, V. Lanticq, and Y. Jaouën, "Enhancement of sensing range of Brillouin optical time-domain reflectometry system up to 150 km with in-line bi-directional erbium-doped fibre amplifications," Electron. Lett. 57, 142–144 (2021).
14. M. A. Soto, G. Bolognini, and F. D. Pasquale, "Analysis of optical pulse coding in spontaneous Brillouin-based distributed temperature sensors," Opt. Express 16, 19097–19111 (2008).
15. M. A. Soto, P. K. Sahu, G. Bolognini, and F. Di Pasquale, "Brillouin-Based Distributed Temperature Sensor Employing Pulse Coding," IEEE Sensors J. 8, 225–226 (2008).
16. F. Wang, C. Zhu, C. Cao, and X. Zhang, "Enhancing the performance of BOTDR based on the combination of FFT technique and complementary coding," Opt. Express 25, 3504–3513 (2017).
17. T. Jostmeier, B. Marx, C. Buntebarth, A. Rath, and W. Hill, "Long-distance botdr interrogator with polarization-diverse coherent detection and power evaluation," in Optical Fiber Sensors, pp. T3–21 (2020).
18. T. Joy, T. Jostmeier, B. Marx, and W. Hill, "Increasing the distance range of repeaterless Brillouin - otdr to 250 km by optical amplification," in Optical Fiber Sensors, pp. W1–3. (2022).
19. P. Eraerds, M. Legré, J. Zhang, H. Zbinden, and N. Gisin, "Photon Counting OTDR: Advantages and Limitations," J. Light. Technol. 28, 952–964 (2010).
20. E. Diamanti, C. Langrock, M. M. Fejer, Y. Yamamoto, and H. Takesue, "1.5 μm photon-counting optical time-domain reflectometry with a single-photon detector based on upconversion in a periodically poled lithium niobate waveguide," Opt. Lett. 31, 727–729 (2006).
21. J. Hu, Q. Zhao, X. Zhang, L. Zhang, X. Zhao, L. Kang, and P. Wu, "Photon-Counting Optical Time-Domain Reflectometry Using a Superconducting Nanowire Single-Photon Detector," J. Light. Technol. 30, 2583–2588 (2012).
22. Q. Zhao, L. Xia, C. Wan, J. Hu, T. Jia, M. Gu, L. Zhang, L. Kang, J. Chen, X. Zhang, and P. Wu, "Long-haul and high-resolution optical time domain reflectometry using superconducting nanowire single-photon detectors," Sci. Reports 5, 10441 (2015).
23. G.-L. Shentu, Q.-C. Sun, X. Jiang, X.-D. Wang, J. S. Pelc, M. M. Fejer, Q. Zhang, and J.-W. Pan, "217 km long distance photon-counting optical time-domain reflectometry based on ultra-low noise up-conversion single photon detector," Opt. Express 21, 24674–24679 (2013).
24. C. Antony, J. Hayes, and P. D. Townsend, "Single-photon detector based long-range fibre-optic distributed temperature sensor," in Optical Instrumentation for Energy and Environmental Applications, pp. ET4D–5. (2012).
25. M. G. Tanner, S. D. Dyer, B. Baek, R. H. Hadfield, and S. Woo Nam, "High-resolution single-mode fiber-optic distributed raman sensor for absolute temperature measurement using superconducting nanowire single-photon detectors," Appl. Phys. Lett. 99, 201110 (2011).
26. J. Gasser, D. Warpelin, F. Bussières, J. Extermann, and E. Pomarico, "Distributed temperature sensor combining centimeter resolution with hundreds of meters sensing range," Opt. Express 30, 6768–6777 (2022).
27. H. Xia, M. Shangguan, G. Shentu, C. Wang, J. Qiu, M. Zheng, X. Xie, X. Dou, Q. Zhang, and J.-W. Pan, "Brillouin optical time-domain reflectometry using up-conversion single-photon detector," Opt. Commun. 381, 37–42 (2016).
28. L. Xia, J. Hu, Q. Zhao, J. Chen, P. Wu, and X. Zhang, "A Distributed Brillouin Temperature Sensor Using a Single-Photon Detector," IEEE Sensors J. 16, 2180–2185 (2016).
29. A. Masoudi, M. Belal, and T. P. Newson, "Distributed dynamic large strain optical fiber sensor based on the detection of spontaneous Brillouin scattering," Opt. Lett. 38, 3312–3315 (2013).
30. I. Quantique, "ID281 Superconducting Nanowire Series," (2023)."